ISSN 1330-3651 (Print), ISSN 1848-6339 (Online)
https://doi.org/10.17559/TV-20190904105201
Original scientific paper

Diagnosis and Location of Open-Circuit Fault in Modular Multilevel Converters Based on High-order Harmonic Analysis

Longzhang KE, Zhenxing LIU, Yong ZHANG

Abstract: Open-Circuit faults of Submodules (SMs) are the most common fault type of modular multilevel converter (MMC). Thus, in order to improve the reliability of MMC, it is very important to detect and locate faulty MMC SMs. In this paper, a new fault diagnosis and location method based on high-order harmonic analysis of the bridge arm voltage is proposed, and the characteristics of SM open-circuit faults are analyzed. In the proposed method, faults are detected by comparing the amplitude of the bridge arm voltage at the switching frequency with a variable threshold, and the phase angle of the bridge arm voltage at the switching frequency is used to locate the faulty SM. The proposed method can detect faulty SM with just one voltage sensor per arm bridge. Moreover, this method can effectively avoid misjudgment of a fault detection signal in the normal transient state. Finally, a MMC model was built using a MATLAB/Simulink environment and simulations were conducted. The experimental results show that the proposed method can not only diagnose a SM fault quickly, but can also locate the faulty SM accurately.

Keywords: fault detection and location; high-order harmonic analysis; modular multilevel converter (MMC); open circuit faults

1 INTRODUCTION

The modular multilevel converter (MMC) was first proposed as a new type of voltage source converter topology by the German scholar R. Marquardt in 2001 [1]. Because of its modular structure and design, easy expansion, high output waveform quality, low operating loss, and common DC bus, it is commonly connected to medium and high voltage direct current and new energy. It is increasingly and widely used in applications such as high voltage electric drives [2-3], high voltage direct current (HVDC) transmissions [4-5].

An MMC comprises a large number of SMs. For example, each bridge arm of the "Trans Bay Cable" project contains 216 SMs [6], and each SM contains two power switching devices, each of which is a potential point of failure. SM faults are one of the common MMC fault types. SM faults lead to deviations between the output voltage and the expected value of a bridge arm, increased inter-phase circulating current, and increased AC and DC side harmonics, which affect the safe and reliable operation of the whole system. After a SM fails, a protection strategy should be adopted immediately. Specific protection strategies should include the following aspects: fast fault detection and location of the faulty SM, fast bypassing of the faulty SM, input of a redundant module, and return of the system to its fault-tolerant operation state [7-8]. Detecting and locating faulty SMs is the premise of fault-tolerant control. Therefore, it is very important to study how to quickly detect faults and accurately locate faulty SMs to ensure safe and stable operation of the system [9-12].

In response to the above problems, much research has been conducted. Reference [13] used a Kalman filter algorithm to compare the difference between measured and estimated values to detect faults, and applied the SM capacitor voltage to locate faulty SMs after failure. The authors of [14] proposed a fault diagnosis method based on the sliding mode observer. Their proposed method effectively diagnoses any open fault of the Insulated Gate Bipolar Transistor (IGBT) and avoids the interference caused by sampling error and system fluctuation. Reference [15] constructed a state observer that can identify multiple SM faults based on the deviation between the measured and calculated values of state variables. In [16], a fault diagnosis and location method based on a mixed kernel support tensor machine was proposed, in which the characteristic data of ac current and internal circulation current are extracted in either normal operation or open-circuit fault. Reference [17] proposed two fault monitoring methods based on a clustering algorithm and on the calculation method of bridge arm equivalent capacitance, which can accurately diagnose and locate faults. Reference [18] identifies faults by determining whether the difference between the predicted and measured values of the bridge arm current exceeds a given threshold. The fault location method is based on the slope of the capacitor voltage of the SM. A series of complete SM fault detection, fault-tolerant control, fault location, and fault reconstruction ideas were proposed in [19], which can achieve fault traversal and improve the reliability of system operation.

This paper proposes a new SM fault diagnosis and localization method based on high-order harmonic analysis of the bridge arm voltage in MMCs. In the proposed method, the amplitude and phase angle of high-frequency harmonic components are used to detect and locate faults. Compared with the methods cited above, the proposed method can detect faults more quickly, significantly reduces the required number of sensors, has no complicated calculations, and is low-cost.

The remainder of this paper is organized as follows. Section II introduces the topology and operating principle of the MMC. Section III analyzes the open-circuit fault characteristics, modulation algorithm, and high-frequency harmonic distribution of MMC SMs, and proposes fault detection based on high-frequency harmonic analysis of the bridge arm voltage in the MMC. Section IV verifies the effectiveness of the proposed method via system simulation results. Finally, Section V presents concluding remarks.

2 MMC TOPOLOGY AND OPERATING PRINCIPLE

2.1 MMC Topology

The three-phase MMC topology is shown in Fig. 1. The MMC consists of three phases and six bridge arms. The upper and lower arms are combined into one phase unit.

Each bridge arm contains one bridge arm reactance and the same number of series SMs.

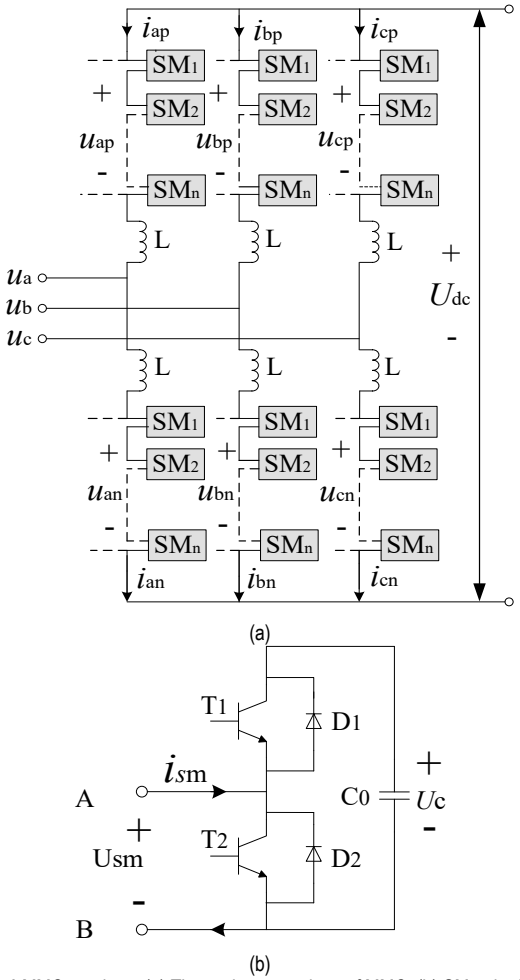

Figure 1 MMC topology: (a) Three-phase topology of MMC; (b) SM unit of MMC

In Fig. 1a, u_a, u_b, u_c are the three-phase AC side voltage of the converter. i_{pj} and i_{nj} are upper and lower arm currents, respectively. u_{jp} and u_{jn} are the upper and lower arm voltages, respectively, where j = a, b, c. I_{dc} is the DC side current, and L is the bridge arm reactance value. Each bridge arm has N SMs connected in series. The SM structure is shown in Fig. 1b. Each SM has two insulated gate bipolar transistors ($T1$ and $T2$), an anti-parallel diode, and a floating capacitor in parallel. u_{sm} is the output voltage of the AC terminal of the SM during steady-state operation. U_{dc} is the DC voltage of the SM. Each bridge arm has an identical bridge arm reactance L in series. The main function of the bridge arm reactance is to suppress the internal circulation between the bridge arms and reduce the current rise rate when the converter fails.

2.2 MMC Operating Principle

The MMC has N SMs per bridge arm and can output up to N + 1 levels. In steady-state operation, the total number of conduction SMs of each phase unit must satisfy Eq. (1). By controlling the number of SMs of the input state in the upper and lower arms, the MMC outputs a multi-level waveform:

$$U_{dc} = N \cdot U_c \tag{1}$$

Table 1 SM Operating Mode and Operating State

SM state	Mode	$T1$	$T2$	i_{sm}	u_{sm}	Capacitor state
CLOSE	1	0	0	positive	U_c	charge
ON	2	1	0	positive	U_c	charge
OFF	3	0	1	positive	0	bypass
CLOSE	4	0	0	negative	0	bypass
ON	5	1	0	negative	U_c	discharge
OFF	6	0	1	negative	0	bypass

There are three kinds of operating states and six operating modes in the steady-state operation of MMC. The operating states are ON state, OFF state, and CLOSE state, as shown in Tab. 1.

ON state: $T1$ is on, $T2$ is off, and the SM is in the ON state, belonging to the normal operating state of MMC.

OFF state: $T1$ is off, $T2$ is on, and the SM is in the OFF state, belonging to the normal operating state of MMC.

CLOSE state: $T1$ and $T2$ are simultaneously turned off. At this time, current flows through $D1$, or current flows through $D2$ to bypass capacitor C, which is generally abnormal operation.

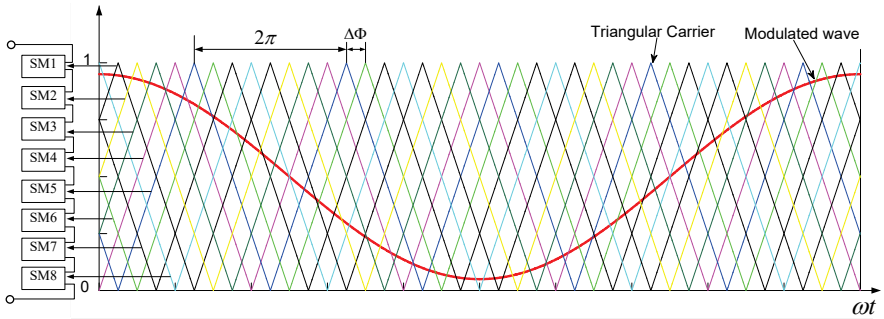

Figure 2 Schematic diagram of CPS-PWM

2.3 MMC Modulation

The modulation strategy of MMC is the key link of the valve control stage. The purpose of the modulation link is to control the ON and OFF states of the converter switching device according to the reference voltage waveform, so that the MMC output AC voltage approaches the reference voltage waveform. At present, the modulation strategies of MMC proposed in the literature mainly include nearest level modulation (NLM), carrier level shifted pulse width modulation (LS-PWM), and carrier phase-shifted modulation (CPS-PWM). This paper focuses on the carrier phase-shift modulation strategy because it can effectively reduce harmonics at lower switching frequencies. The

reference voltages of the SMs are the same, which is beneficial to the balance of the capacitor voltage. Most importantly, it is applied in the SM fault detection and localization algorithm presented in Section III.

N sets of triangular carriers with frequency f_c are required for MMCs with N cascaded SMs, and the phase angles are sequentially shifted by $\Delta\emptyset = 2\pi/N$. Assuming that the reference voltage of the bridge arm is u^*_{arm} and the reference voltage for module i is $u^*_{sm\_i}$, the reference voltage of each SM should be equal to the bridge reference voltage, which is $u^*_{sm\_i} = u^*_{arm}$. The N SMs reference voltages are compared with the N sets of carriers to generate N sets of PWM pulses to respectively control the upper IGBTs of the N SMs, and the lower IGBTs of the N SMs are controlled by adding a certain dead time. The CPS-PWM principle is shown in Fig. 2. The switching frequency of each SM is $f_s = f_c = 1/T$. Fig. 2 shows the eight phase-shifted carriers and a modulated wave waveform. Fig. 3 shows the bridge voltage waveform corresponding to Fig. 2, which is the sum of two-level PWM voltages output by eight SMs.

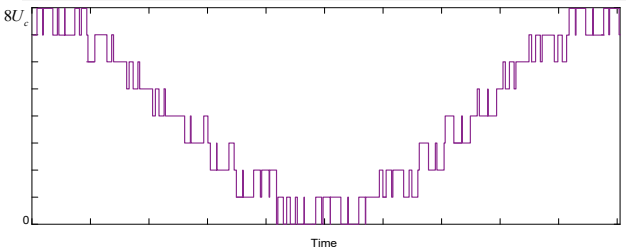

Figure 3 Bridge arm voltage waveform

The output voltage of the bridge arm is the superposition of the two-level PWM pulse voltage of all SMs. The sum of the reference voltages of all SMs of the bridge arm should be equal to N times the reference voltage of the bridge arm, as follows:

$$\sum_{i=1}^{N} u^*_{sm\_i} = N \cdot u^*_{arm} \tag{2}$$

Eq. (2) is a constraint condition to ensure that the output characteristics of the bridge arm remain unchanged. As long as Eq. (2) is satisfied, the reference voltage of each SM in the bridge arm can be adjusted in a small range without changing the output voltage of the whole bridge arm, and the capacitance voltage can be balanced.

3 FAULT DIAGNOSIS AND LOCATION METHOD OF MMC

The semiconductor devices in the SMs of MMC are relatively fragile, and the number of IGBTs in practical projects is relatively large. Therefore, an IGBT in a SM may be damaged because of overvoltage, overcurrent, or other reasons. SM faults can be divided into two types: short-circuit faults and open-circuit faults. Short-circuit faults have mature solutions, whereas open-circuit faults for a power device are not obvious, are not easily discovered, and their impact is greater. Therefore, this paper focuses primarily on open-circuit faults of SMs.

3.1 Open-circuit Fault Analysis of SMs

In studying the AC side output voltage characteristics of SMs, the output voltage of a SM can be expressed as follows:

$$u_{sm} = S_i \cdot U_c(i) \tag{3}$$

where S_i is the switch function of the SM. The output voltage of the SM in normal and faulty conditions is shown in Tab. 2.

When an open-circuit fault occurs in $T1$, if $T1$ is in the OFF state, the open-circuit fault has no effect on the OFF state. When an open-circuit fault occurs in $T1$ and $T1$ is in the ON state, at $i_{sm} > 0$, the bridge arm current path is as shown in Fig. 4a. The capacitor can be charged normally, and the output voltage of the SM is u_{sm}. At $i_{sm} < 0$, the bridge arm current is as shown in Fig. 4b. In this case, the output voltage of the SM is zero and the capacitor cannot discharge normally.

When an open-circuit fault occurs in $T2$ and $T2$ is in the ON state, the open-circuit fault has no effect on the OFF state. When $T2$ is in the ON state, at $i_{sm} < 0$, the bridge arm current path is as shown in Fig. 4b. The output voltage is the same as normal in this case. At $i_{sm} > 0$, the bridge arm current is as shown in Fig. 4a. In this case, the output voltage of the SM differs by U_c from that of the normal state. Obviously, open-circuit faults in $T1$ and $T2$ have different effects on the charging and discharging of MMC SMs. An open-circuit fault in $T1$ only affects the discharging mode in the ON state of SMs because an open circuit in $T1$ causes SMs to be bypassed and cannot discharge normally. An open-circuit fault in $T2$ only affects the bypass mode in the OFF state of SMs, causing SMs to be charged but not bypassed.

Whether an open-circuit fault occurs in $T1$ or $T2$, it will eventually lead to increased capacitance voltage in a faulty SM.

3.2 High Harmonic Analysis of CPS-PWM

In Sinusoidal pulse width modulation (SPWM) mode, the output PWM voltage waveform is determined by the modulation wave frequency and the carrier frequency. Each SM is equivalent to a two-level converter. The output two-level PWM voltage waveform of each SM is analyzed by the double Fourier transform method [20]. Using two-level natural sampling, the harmonic distribution expression of the output voltage of the SM can be obtained as follows:

$$u_{sm\_i} = \frac{U_c}{2} M \cos(\omega_1 t + \theta_1) + \frac{U_c}{2} \sum_{m=1}^{\infty} \sum_{n=-\infty}^{\infty} C_{mn(SM)} \cdot \cdot \cos\left[m(\omega_{c1} t + \theta_{c1}) + i\frac{2\pi}{N} + n(\omega_1 t + \theta_1) \right] \tag{4}$$

where i is the SM number, and $i = 1, 2, \ldots, N$, m is a multiple of carrier frequency and n is a multiple of fundamental frequency. θ_1 is the initial phase of the modulated wave, θ_{c1} is the initial phase of the carrier wave.

In Eq. (4), the harmonic amplitude coefficient of the output voltage of SM can be written as:

$$C_{mn(\mathrm{SM})}=\frac{4}{m\pi}\sin\left[(m+n)\frac{\pi}{2}\right]J_n\left(m\frac{\pi}{2}M\right) \tag{5}$$

where M is the modulation ratio, $J_n(x)$ is the n-order Bessel function, m is a multiple of carrier frequency and n is a multiple of fundamental frequency. From the expression of harmonic distribution of u_{sm}, it can be seen that the harmonic of the two-level PWM voltage is mainly distributed in the fundamental frequency band, carrier frequency band, and carrier sideband, which can be written in the form $m\omega_{\mathrm{c}}\pm n\omega_1$.

Table 2 Output voltage of SMs in normal and faulty conditions

Condition	Normal	$T1$ in open state	$T2$ in open state
$S=1$ & $i_{\mathrm{sm}}<0$	$u_{\mathrm{sm}}=U_{\mathrm{c}}$	$u_{\mathrm{sm}}=0$	$u_{\mathrm{sm}}=U_{\mathrm{c}}$
$S=1$ & $i_{\mathrm{sm}}>0$	$u_{\mathrm{sm}}=U_{\mathrm{c}}$	$u_{\mathrm{sm}}=U_{\mathrm{c}}$	$u_{\mathrm{sm}}=U_{\mathrm{c}}$
$S=1$ & $i_{\mathrm{sm}}<0$	$u_{\mathrm{sm}}=0$	$u_{\mathrm{sm}}=0$	$u_{\mathrm{sm}}=0$
$S=1$ & $i_{\mathrm{sm}}<0$	$u_{\mathrm{sm}}=0$	$u_{\mathrm{sm}}=0$	$u_{\mathrm{sm}}=U_{\mathrm{c}}$
$S=1$ & $i_{\mathrm{sm}}<0$	$u_{\mathrm{sm}}=U_{\mathrm{c}}$	$u_{\mathrm{sm}}=0$	$u_{\mathrm{sm}}=U_{\mathrm{c}}$

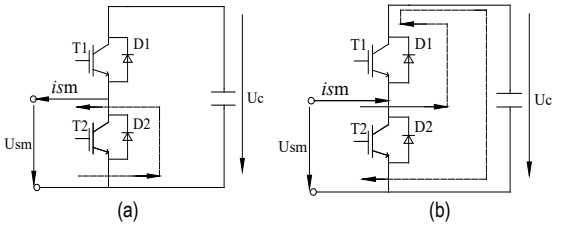

Figure 4 Current path in SM open-circuit fault: (a) $i_{\mathrm{sm}}>0$; (b) $i_{\mathrm{sm}}<0$

For Eq. (4), the following relationship is established:

$$\sum_{i=1}^{N}\cos\left[m(\omega_{\mathrm{c}}t+\theta_{\mathrm{c1}})+i\frac{2\pi}{N}+n(\omega_1t+\theta_1)\right]=\begin{cases}0 & m\neq kN\\ N\cos\left[m(\omega_{\mathrm{c}}t+\theta_{\mathrm{c1}})+i\frac{2\pi}{N}+n(\omega_1t+\theta_1)\right] & m=kN\end{cases} \tag{6}$$

Where k = 1, 2, …, ∞ and the total voltage of the bridge arm is equal to the sum of the output two-level PWM voltage of N SMs on the bridge arm. The expression of the bridge arm voltage is as follows:

$$u_{\mathrm{arm}}=\frac{U_{\mathrm{dc}}}{2}M\cos(\omega_1t+\theta_1)+\sum_{m=1}^{\infty}\sum_{n=-\infty}^{\infty}\frac{U_{\mathrm{dc}}}{2}\times C_{mn(\mathrm{ps})}\cos[m(N\omega_{\mathrm{c}}t+N\theta_{\mathrm{c1}})+n(\omega_1t+\theta_1)] \tag{7}$$

In Eq. (7), the amplitude coefficient of the bridge arm voltage harmonic can be written as follows:

$$C_{mn(\mathrm{ps})}=\frac{4}{\pi}\frac{1}{mN}\sin\left[(mN+n)\frac{\pi}{2}\right]J_n\left(mN\frac{\pi}{2}M\right) \tag{8}$$

It can be seen from Eqs. (4) to (7) that when the CPS-PWM method is adopted, the carrier frequency band and its sideband harmonic components whose carrier multiple is a non-N integer times the output voltage by each SM on the same bridge arm are all cancelled by the CPS-PWM technology in the process of waveform superposition.

From the expression of the bridge arm voltage harmonic distribution, the CPS-PWM strategy is equivalent to raising the original two-level PWM carrier frequency ω_{c} to $N\omega_{\mathrm{c}}$. That is, the equivalent carrier frequency of the final multi-level PWM voltage is $\omega_{\mathrm{c}}=N\omega_{\mathrm{c1}}$. The harmonics are also distributed in the corresponding carrier frequency band and its sideband with this equivalent carrier frequency.

3.3 Detection Principle of Open-circuit Fault for SM

Reference [21] proposed a fault detection method for FC converter based on harmonic frequency analysis. In this method, faults are detected by analyzing the amplitude of the output phase voltage of the converter at the switching frequency. In MMC, the amplitude of the switching frequency component should be zero in theory due to the carrier phase shift. According to the carrier phase-shifted harmonic distribution expression in Section III-B, the output voltage of each SM at f_{s} can be expressed by a phasor $\vec{V}_{si}$, where the amplitude is $\left|\vec{V}_{si}\right|$ and the initial phase is

$$\phi_i=-(i-1)\Delta\phi\quad i=1,2,3,...,N \tag{9}$$

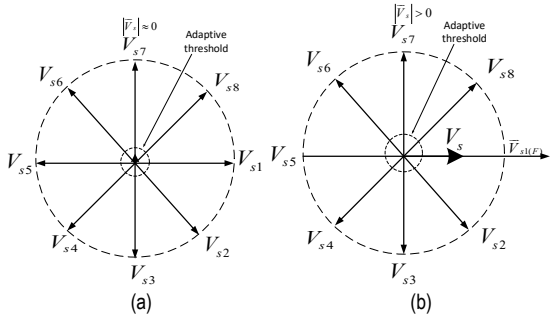

Figure 5 Phasor diagram: (a) normal operation; (b) fault condition on SM1

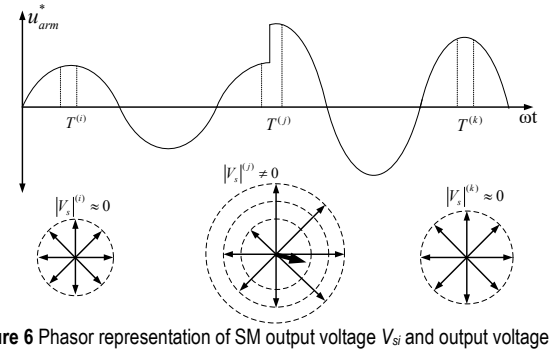

Figure 6 Phasor representation of SM output voltage V_{si} and output voltage V_{s}

As can be seen from Eq. (8), this corresponds to the initial carrier phase of each SM. Fig. 5 is a phasor diagram of the bridge arm voltage at switching frequency f_{s} for a 9-level MMC under normal and SM fault conditions.

Eq. (2) shows that the bridge arm voltage is equal to the sum of the actual output voltage of each SM, and the switching frequency component of the bridge arm voltage is the resulting switching frequency component $\vec{V}_{\mathrm{s}}$, which is equal to the superposition of the frequency component f_{s}

of the output voltage of each SM in the bridge arm. This can be expressed as follows:

$$\left|\vec{V}_{\mathrm{s}}\right|=\left|\sum_{i=1}^{N}\left|\vec{V}_{si}\right|\mathrm{e}^{j\phi_i}\right| \tag{10}$$

As a result of the symmetry of each SM unit, under normal conditions, the corresponding amplitude of switching frequency component should be zero:

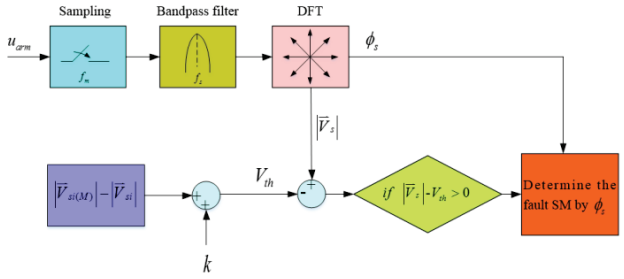

Figure 7 Flowchart of the fault diagnosis strategy implementation scheme

$$\vec{V}_{\mathrm{s}}=\sum_{i=1}^{N}\vec{V}_{si}\approx 0 \tag{11}$$

$$\left|\vec{V}_{\mathrm{s}}\right|=\sum_{i=1}^{N}\left|\vec{V}_{si}\right|=\left|\vec{V}_{si(F)}\right|-\left|\vec{V}_{si}\right|>0 \tag{12}$$

where $\left|\vec{V}_{si(F)}\right|$ is the amplitude of the output voltage of the fault SM at switching frequency f_s.

When a SM fails, as analyzed in Section III-A, the output voltage of the fault SM will increase. $\left|\vec{V}_{si(F)}\right|$ will also increase, while the output voltage of other normal SMs on the bridge arm will remain unchanged. As shown in Fig. 5b, $\left|\vec{V}_{si(F)}\right|$ ill be greater than the amplitude $\left|\vec{V}_{si}\right|$ corresponding to the output voltage switching frequency of the SM when it is in the normal state.

Compared with the normal state, the switching frequency f_s and its integral multiple harmonic component are no longer zero after the fault. $\left|\vec{V}_{\mathrm{s}}\right|$ will be greater than zero, and the phasor is $\angle\vec{V}_{\mathrm{s}}=\angle\vec{V}_{si(F)}$. This phase is used to locate the faulty SM. Therefore, by detecting the amplitude and phase of the bridge arm voltage at switching frequency, it is possible to detect and locate any faulty SM on the bridge arm.

3.4 Threshold

The amplitude of the resulting switching frequency component $\vec{V}_{\mathrm{s}}$ is approximately equal to zero in the steady state. A small component of the switching frequency is always present in the steady state owing to dead times and ripples. In addition, system transient conditions can also cause a significant increase in the switching frequency amplitude. As shown in Fig. 6 to accurately distinguish between normal transient conditions and SM fault conditions, it is important to set a threshold for fault detection.

According to the analysis in Section III-B, the harmonic frequency amplitude coefficient of u_{sm} is C_{mn}. When $m = 1$ and $n = 0$, it is the switching frequency amplitude coefficient $C_{1,0}$ from which Eq. (16) follows:

$$\left|\vec{V}_{si}\right|=C_{1,0}=\frac{4}{\pi}\sin\frac{\pi}{2}J_n\left(M\frac{\pi}{2}\right) \tag{13}$$

In steady state, $\left|\vec{V}_{si}\right|$ is mainly affected by modulation ratio M. Considering the influence of dead time and system ripple on the switching frequency component, the threshold needs to be added with a small DC offset to overcome its effect. The final threshold is a variable that varies with the modulation ratio M:

$$V_{\mathrm{th}}=\left(\left|\vec{V}_{si(M)}\right|-\left|\vec{V}_{si}\right|\right)+k=\frac{4}{\pi}J_n\left(\Delta M\frac{\pi}{2}\right)+k \tag{14}$$

where $\left|\vec{V}_{si(M)}\right|$ is the amplitude of output voltage of the SM at f_s in transient state.

3.5 Implementation

The implementation scheme of fault detection and location is as follows. According to the harmonic distribution characteristics of CPS-PWM modulation strategy and the time domain sampling theorem, in order to analyze the frequency component at the equivalent switching frequency Nf_s, the sampling frequency f_m is greater than or equal to twice the equivalent switching frequency, and the DFT algorithm is used to extract the amplitude and phase of the bridge arm voltage at the switching frequency f_s:

$$\vec{V}_{\mathrm{s}}(t)=\frac{2}{n}\sum_{i=1}^{n-1}u_{\mathrm{arm}}\left(t-\frac{i}{f_m}\right)\cdot\mathrm{e}^{\frac{j2\pi i}{n}} \tag{15}$$

$$\phi_s=\arctan\left(\frac{\mathrm{Im}(\vec{V}_s)}{\mathrm{Re}(\vec{V}_s)}\right) \tag{16}$$

Table 3 MMC simulation parameters

Parameter	Value
Rated DC Voltage	8 kV
Number of SMs per arm	8
Line frequency	50 Hz
Carrier switching frequency	1000 Hz
SM capacitance	4.7 mF
Arm inductance	5 mH
Carrier ratio	20

After the bridge arm voltage is collected, the sideband component of f_s in the bridge arm voltage is filtered by a bandpass filter with a center frequency of f_s. Finally, the amplitude of the output voltage at switching frequency calculated by the DFT algorithm is compared with the fault detection threshold value. If $\left|\vec{V}_{\mathrm{s}}\right|>V_{\mathrm{th}}$, the SM is determined to be faulty. The phase angle extracted by DFT is used to locate the faulty SM. Once the faulty SM is located, the by-pass switch of the SM is closed

immediately, and the system enters the fault-tolerant control state. The flowchart of the fault diagnosis strategy implementation scheme is shown in Fig. 7.

4 SIMULATION EXPERIMENT

A 9-level MMC simulation model was built in a MATLAB/Simulink environment. The simulation parameters are shown in Tab. 3.

4.1 Spectrum Analysis

Fig. 8 shows the spectrum distribution of the output voltage waveform of the SM. It can be seen from Fig. 8 that the higher harmonics of the output voltage waveform of the SM are mainly concentrated in the odd times carrier frequency band and its sideband harmonics, as well as the even times carrier sideband, while the most serious harmonics caused by the modulation strategy are at the carrier frequency f_c.

The spectrum distribution of the bridge arm voltage waveform is shown in Fig. 9. It is obvious that the bridge arm voltage waveform no longer contains carrier f_c and its sideband harmonics.

The spectrum distribution of the bridge arm voltage after the fault of the SM is shown in Fig. 10. Compared with Fig. 9, the switching frequency f_s and its integral harmonic component are no longer zero after the fault.

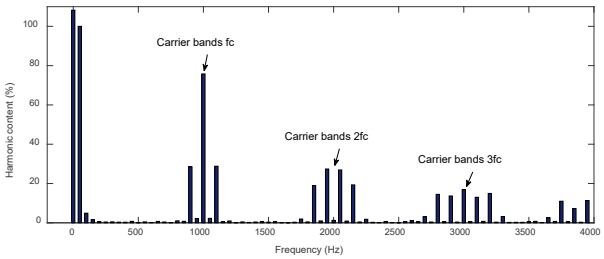

Figure 8 Spectrum distribution diagram of the bridge arm voltage in normal condition

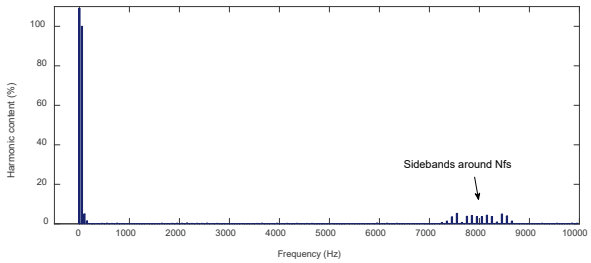

Figure 9 Spectrum distribution diagram of the output voltage of the SM in normal condition

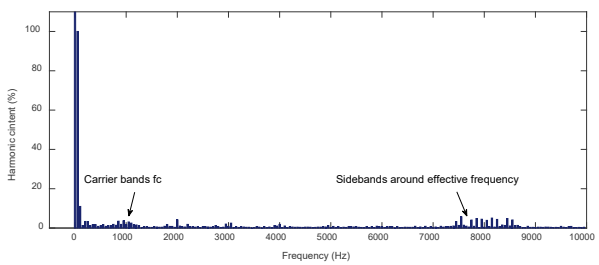

Figure 10 Spectrum distribution of the bridge arm voltage in SM fault condition

4.2 Simulation Results

Fig. 11 shows the voltage and current waveform of the bridge arm. When the modulation ratio changes from M = 0.68 to M = 0.98, the voltage of the bridge arm increases. In Fig. 11c, at t = 0.3 s, the modulation ratio has a step change. At this time, $\overline{V}_s$ has a small spike change at the switching frequency. According to Eq. (13), the threshold also adaptively changes stepwise with the modulation ratio, avoiding the misjudgment of the fault detection signal.

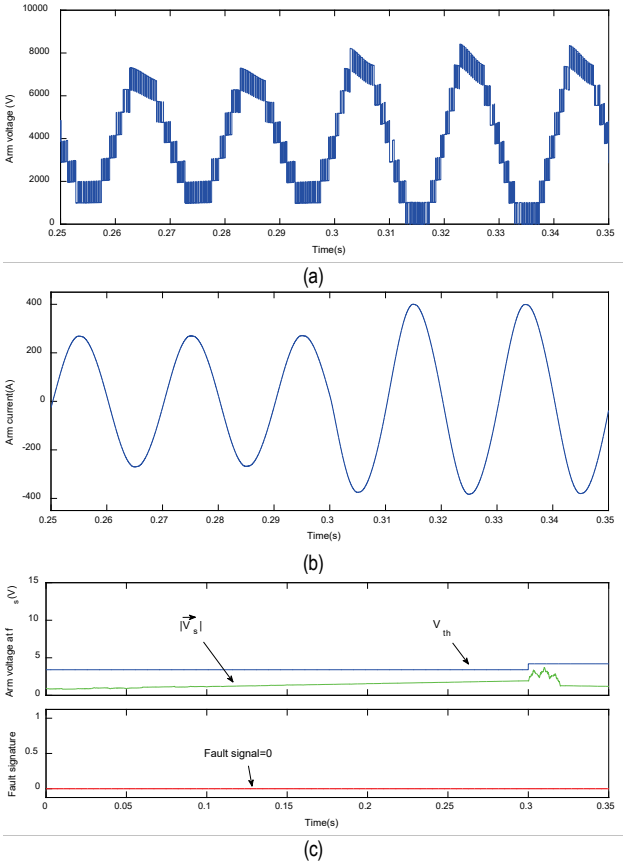

Figure 11 Simulation verification under modulation ratio conversion conditions at t = 0.3 s: (a) Output voltage of bridge arm; (b) Load phase current; (c) Magnitude of $\overline{V}_s$ in comparison with V_{th}

As shown in Fig. 12, an open-circuit fault occurs on SM2 at t = 0.4 s. in Fig. 12a, the voltage waveform of the bridge arm is distorted and a level is lost. The corresponding load phase current waveform is shown in Fig. 12b. In Fig. 12c, according to the analysis in Section III-C, the output voltage of the fault SM increases at the switching frequency; thus, as $\overline{V}_s$ is no longer zero, it is compared with the threshold value, and the fault detection flag signal quickly detects the occurrence of the fault after a 2.5 ms delay.

In Fig. 13a, the output voltage of the AC side of the SM increases after the fault occurs, which is consistent with the analysis in Section III-A. The waveform after bandpass filtering at the center frequency of f_s is shown in Fig. 13b.

Fig. 14 is a phasor diagram of switching frequency amplitude and phase angle of the bridge arm extracted with DFT algorithm after faults on SM1 and SM2. It can be clearly seen from the phasor diagram that after the faults

occurrence on SM1 to SM8, the phase angles of $\overrightarrow{V_s}$ correspond to −45° and −90°, respectively, and after the other SMs fails, the phase angles are −135°, 180°, 135°, 90°, 45° and 0°, respectively. For MMC converters with more SMs per arm, the same method can be used to locate the faulty SMs accurately.

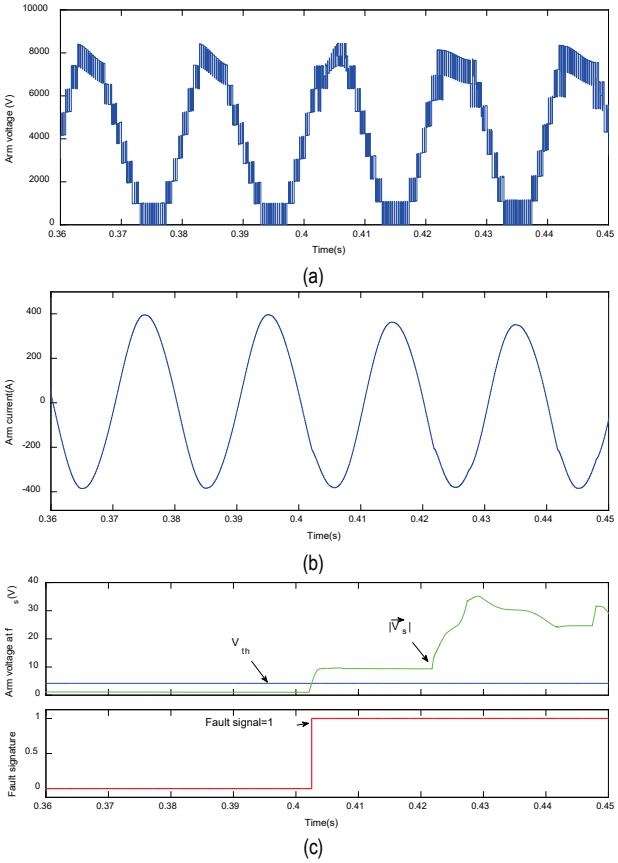

Figure 12 Simulated behavior under the open-circuit fault condition at t = 0.4 s: (a) Output voltage of bridge arm; (b) Load phase current; (c) Magnitude of $\overrightarrow{V}_s$ in comparison with V_{th}

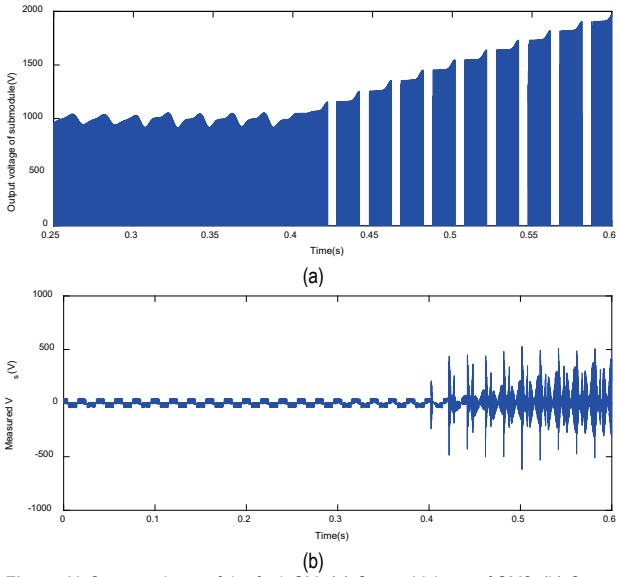

Figure 13 Output voltage of the fault SM: (a) Output Voltage of SM2; (b) Output voltage after bandpass filtering

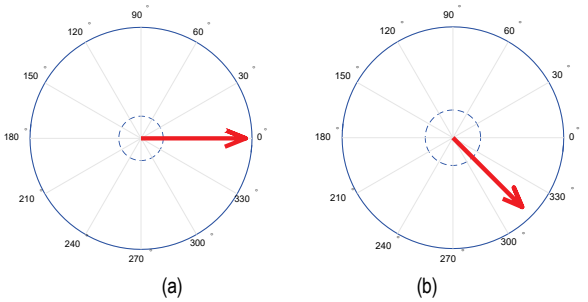

Figure 14 Phasor $\overrightarrow{V}_s$ representation: (a) Fault on SM1; (b) Fault on SM2

5 CONCLUSION

In this paper, a fault detection method based on high-order harmonic analysis of the MMC bridge arm voltage was proposed. In the proposed method, the amplitude and phase angle of the bridge arm voltage at switching frequency are obtained by collecting the voltage of the MMC bridge arm, and performing filtering and DFT transformation. Then, by comparing the amplitude of output bridge arm voltage at switching frequency with a threshold value varying with the modulation ratio, the normal transient state and the fault state are effectively distinguished. Subsequently, according to the characteristics of harmonic distribution of the CPS-PWM method, the phase angle corresponding to the switching frequency component is calculated to locate the faulty SM. Simulation results show that the fault diagnosis method proposed in this paper cannot only detect faults quickly, but can also locate faults accurately, because it takes high-frequency harmonics as the detection object, and can monitor the change of amplitude in a short time (2.5 ms). For the entire MMC converter, only six voltage sensors are needed, which reduces cost and detection complexity, and is easy to implement. This method lays the foundation for the next step of fault-tolerant control. Future research will focus on the diagnosis of specific switching devices on SMs in MMC.

6 REFERENCES

[1] Lesnicar, A. & Marquardt, R. (2003). An innovative modular multilevel converter topology suitable for a wide power range. *Proc. IEEE Power Tech. Conf.*, 1-6. https://doi.org/10.1109/PTC.2003.1304403

[2] Debnath, S., Qin, J., Bahrani, B., Saeedifard M., & Barbosa, P. (2015). Operation, control, and applications of the modular multilevel converter: A review. *IEEE Trans. Power Electronics, 30*(1), 37-53. https://doi.org/10.1109/TPEL.2014.2309937

[3] Deng, F. & Chen, Z. (2015). Voltage-balancing method for modular multilevel converters under phase-shifted carrier-based pulse-width modulation. *IEEE Trans. Ind. Electron., 62*(7), 4158-4169. https://doi.org/10.1109/TIE.2014.2388195

[4] Hagiwara, M., Hasegawa, I., & Akagi, H. (2013). Start-up and low-speed operation of an electric motor driven by a modular multilevel cascade inverter. *IEEE Trans. Ind. Appl., 49*(4), 1556-1565. https://doi.org/10.1109/TIA.2013.2256331

[5] Jo, Y. J., Nguyen, T. H., & Lee, D. C. (2016). Capacitance estimation of the submodule capacitors in modular multilevel converters for HVDC applications. *Journal of Power Electronics, 16*(5), 1752-1762. https://doi.org/10.6113/JPE.2016.16.5.1752

[6] Tu, Q., Xuand, Z., & Xu, L. (2011). Reduced switching-frequency modulation and circulating current suppression for modular converters (MMC). *IEEE Trans. Power Del., 26*(3), 2009-2017. https://doi.org/10.1109/TPWRD.2011.2115258

[7] Hu, P., Jiang, D., Zhou, Y., Liang, Y., Guo, J., & Lin, Z. (2014). Energy-balancing control strategy for modular multilevel converters under SM fault conditions. *IEEE Trans. Power Electronics, 29*(9), 5021-5030. https://doi.org/10.1109/TPEL.2013.2284919

[8] Li, B., Wang, G., & Xu, D. (2016). Modulation, Harmonic Analysis, and Balancing Control for a New Modular Multilevel Converter. *Journal of Power Electronics, 16*(1), 163-172. https://doi.org/10.6113/JPE.2016.16.1.163

[9] Song, Q., Liu, W., Li, X. et al. (2013). A steady-state analysis method for a modular multilevel converter. *IEEE Transaction of Power Electronics, 28*(8), 3702-3713. https://doi.org/10.1109/TPEL.2012.2227818

[10] Haghnazari, S., Khodabandeh, M. et al. (2016). Fast fault detection method for modular multilevel converter semiconductor power switches. *IET Power Electronics, 9*(2), 165-174. https://doi.org/10.1049/iet-pel.2015.0392

[11] Wang, J., Ma, H., & Z. Bai. (2018). A submodule fault ride-through strategy for modular multilevel converters with nearest level modulation. *IEEE Trans. Power Electronics, 33*(2), 1597-1608. https://doi.org/10.1109/TPEL.2017.2679439

[12] Picas, R., Pou, J., & Ceballos, S. (2017). Reliable modular multilevel converter fault detection with redundant voltage sensor. *IEEE Trans. Power Electronics, 32*(1), 39-51. https://doi.org/10.1109/TPEL.2016.2526684

[13] Deng F., Chen, Z., Khan, M. R., & Zhu, R. (2015). Fault detection for modular multilevel converters. *IEEE Trans. Power Electronics, 30*(5), 2721-2732. https://doi.org/10.1109/TPEL.2014.2348194

[14] Shao, S., Wheeler, P. W., Clare, J. C., & Watson, A. J. (2013). Fault detection for modular multilevel converters based on sliding mode observer. *IEEE Trans. Power Electronics, 28*(11), 4867-4872. https://doi.org/10.1109/TPEL.2013.2242093

[15] Shao, S., Watson, A. J., Clare, J. C., & Wheeler, P. W. (2016). Robustness analysis and experimental validation of a fault detection and isolation method for the modular multilevel converter. *IEEE Trans. Power Electron*ics, 31(5), 3794-3805. https://doi.org/10.1109/TPEL.2015.2462717

[16] Li, C., Liu, Z., Zhang, Y., Chai L., & Xu, B. (2019). Diagnosis and location of the open-circuit fault in modular multilevel converters: An improved machine learning method. *Neurocomputing, 331*, 58-66. https://doi.org/10.1016/j.neucom.2018.09.041

[17] Yang, Q., Jiang, C., & Saeedifard, M. (2016). Analysis, detection, and location of open-Switch SMfailures in a modular multilevel converter. *IEEE Trans. Power Deliv.,* 31(11), 155-164. https://doi.org/10.1109/TPWRD.2015.2477476

[18] Xu, K. & Xie, S. (2018). Fault diagnosis method for SMs failures in MMCs based on improced incremental predictive model of arm current. *Journal of Power Electronics, 18*(5), 1608-1617.

[19] Li, B., Shi, S., Wang, B., Wang, G., & Xu, D. (2016). Fault diagnosis and tolerant control of single IGBT open-circuit failure in Modular Multilevel Converter. *IEEE Trans. Power Electronics, 31*(11), 3165-3176. https://doi.org/10.1109/TPEL.2015.2454534

[20] Holmes, D. G. & McGrath, B. P. (2001). Opportunities for harmonic cancellation with carrier-based PWM for two-level and multilevel cascaded inverters. *IEEE Trans. Ind. Appl., 37*(2), 574-582. https://doi.org/10.1109/28.913724

[21] Richardeau, F., Baudesson P., & Meynard, T. A. (2002). Failure-tolerance and remedial strategies of a PWM multicell inverter. *IEEE Trans. Power Electron*ics*, 17*(6), 905-912. https://doi.org/10.1109/TPEL.2002.805588

Contact information:

Longzhang KE
School of Information Science and Engineering,
Wuhan University of Science and Technology,
Wuhan 430081, China
School of Electromechanical and Automobile Engineering,
Huanggang Normal University,
Huanggang 438000, China
E-mail: kelongzhang@hgnu.edu.cn

Zhenxing LIU
(Corresponding author)
School of Information Science and Engineering,
Wuhan University of Science and Technology,
Wuhan 430081, China
E-mail: zhenxingliu@wust.edu.cn

Yong ZHANG
School of Information Science and Engineering,
Wuhan University of Science and Technology,
Wuhan 430081, China
E-mail: zhangyong77@wust.edu.cn